Transactions, SMiRT-23
Manchester, United Kingdom - August 10-14, 2015
Division II

Sensitivity studies on numerical J-integral assessment of specimens containing dissimilar metal welds

Igor Simonovski[1], Oliver Martin[1]

[1] European Commission, DG JRC, Institute for Energy and Transport, The Netherlands

ABSTRACT

In 2012 a research project MULTIMETAL was started within the 7th Framework Programme for Research and Technological Development of the European Union. The aim of the project is to develop a standard for measuring the fracture resistance of multi-metallic specimen and the development of harmonized procedures for dissimilar metal welds (DMWs) brittle and ductile integrity assessment. DMWs connect ferritic and austenitic stainless steels and are present at a number of locations in light water reactors primary piping systems. This paper presents a sensitivity analysis of the influential modelling parameters for the SEN(B) and SEN(T) specimens containing various DMW material zones that were used within the numerical benchmark: 'Numerical Analyses of DMW Behaviour'. Sensitivity to the J-integral and η_{pl} values is ascertained.

INTRODUCTION

At the moment there is no existing standard for the fracture resistance testing of multi-metallic components or specimens that are made up of different material sections joined together via a weld. Existing standards for fracture resistance testing like ASTM E1820-13 ASTM (2013), ISO 12135:2002 ISO (2002) and engineering procedures or schemes like DNV DNV (2006) for the estimation of J-integral values are intended for specimens made of homogeneous material only. Thus in early 2012 a group of 11 European organisations started a R&D project MULTIMETAL MULTIMETAL (2012) with the aim of filling the above gaps. The objectives of the project are the development of a standard for fracture resistance testing of multi-metallic specimens and the development of harmonized procedures for dissimilar metal welds (DMWs) brittle and ductile integrity assessment. DMWs are typically present in safe-ends of LWRs primary circuits. The underlying aim of MULTIMETAL is to provide recommendations for a good practice approach for the integrity assessment of DMWs as part of overall integrity analyses and leak-before-break (LBB) procedures. The project was funded by the European Commission (EC) within its 7th Framework Program and concluded in January 2015. This paper presents a sensitivity analysis of the influential modelling parameters for the SEN(B) and SEN(T) specimens containing various DMW material zones that were used within the numerical benchmark: 'Numerical Analyses of DMW Behaviour'. Sensitivity to the J-integral and η_{pl} values is ascertained.

SPECIMENS

Specimens are based on a mock-up of a DMW from the primary circuit of the European Pressurized Water Reactor (EPR). The mock-up is labeled as MU1 and resembles an existing DMW in terms of geometry, material and weld procedure. The MU1 consists of an austenitic stainless steel plate, a ferritic steel plate and a weld between the two plates, see Fig. 1. It is a narrow gap, no buttering weld with Inconel 52 as filler material. This mock-up continues the work of the STYLE STYLE (2010) and ADIMEW Faidy (2015) projects that dealt with improving the LBB assessment procedures for DMWs. Post-weld heat treatment has been performed on the MU1 and an extensive material characterization has been performed Bourgeois et al. (2015a,b,c); Keinänen et al. (2015). Fig. 2 shows the corresponding room-temperature stress-strain data for different materials. Adjacent materials have different yield stresses and hardening which affects the strain concentrations and results in unsymmetrical response of the fracture specimens.

CT, SEN(B) and SEN(T) specimens were cut out of the MU1. In case of MU1 specimens, the crack is usually placed on the fusion line between the Ferritic Steel-Heat Affected Zone (FS-HAZ) and Weld Metal (WM) or slightly inside the WM. This is based on the STYLE and ADIMEW studies which showed that this interface is the weakest area in terms of toughness Bourgeois et al. (2015c). For the purpose of this paper only two specimens are used: a) SEN(B)20x20 with a crack placed 0.5 mm from the fusion line in the direction of the weld metal and b) SEN(T)20x20 with a crack placed at the fusion line. In each case a crack length of a/W=0.6 is used. Fig. 3 shows the corresponding finite elements models with boundary conditions and material zones.

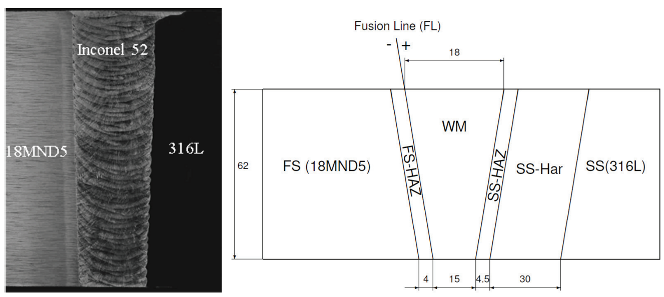

Figure 1: MU1. All the dimensions are in mm.

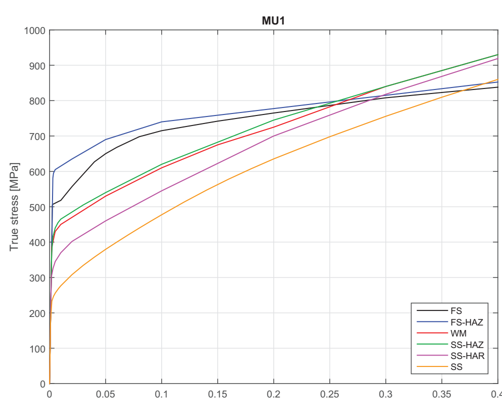

Figure 2: True stress-strain curves for different materials in the MU1.

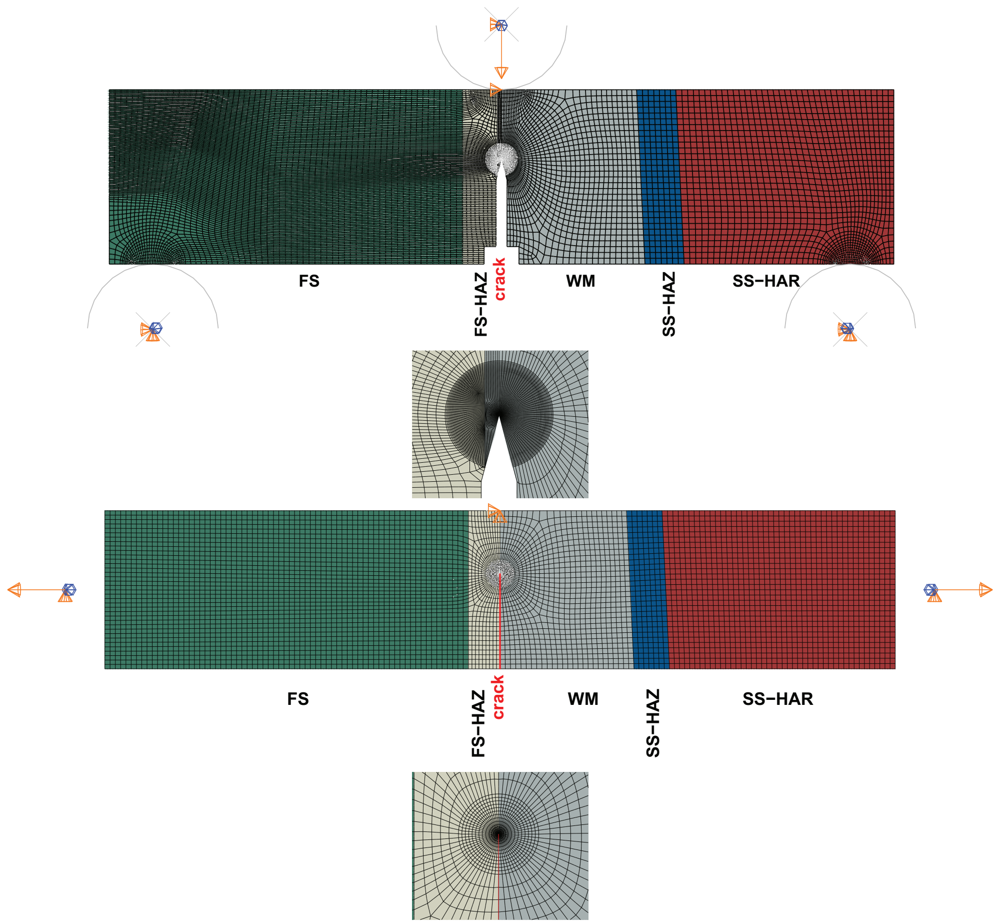

Figure 3: Finite element models of the specimens, including the material zones and boundary conditions. Top: SEN(B). Bottom: SEN(T).

NUMERICAL ANALYSIS

J-integral and η_{pl} values were calculated for a matrix of 2D cases, exploring the influence of individual parameters. J-integral values were computed using finite element (FE) analyses Systemes (2014). The original J-integral definition is valid only for homogeneous materials and is path independent. For inhomogeneous materials a contribution due to the material inhomogeneity (C_{inh}) needs to be added, Eq. (1) Brocks and Scheider (2001); Kikuchi and Miyamoto (1982). However, if the phase boundary between the two materials is parallel to the crack line, the additional contribution C_{inh} becomes zero Brocks and Scheider (2001); Kolednik et al. (2005); Simha et al. (2003). This is true in all our cases. One needs to make sure that the contours don't cross further away interfaces that are not parallel to the crack line.

$$J_i = J_{homog} + C_{inh} = \underbrace{\oint_{\Gamma} [wn_i - \sigma_{ij} n_k u_{j,i}]\, ds}_{J_{homog}} - \underbrace{\oint_{\Gamma_{pb}} [wn_i - \sigma_{ij} n_k u_{j,i}]\, ds}_{C_{inh}} \tag{1}$$

The computed J-integral values were split into elastic and plastic part, Eq. (2), in line with ASTM E1820-13 ASTM (2013). η_{pl} dimensionless correction factors were then computed. The following definition of LLD values were used for computing η_{pl} values: SEN(B)-displacement of the point underneath the top pin and SEN(T)-opening of the crack at the bottom edge of the specimen.

$$J = J_{el} + J_{pl}, \qquad J_{pl} = \frac{\eta_{pl} A_{pl}}{B_N b_o}, \qquad \eta_{pl} = \frac{J_{pl} B_N b_o}{A_{pl}} \tag{2}$$

Initial validation of the models was performed by comparing J-integral and η_{pl} values using homogeneous cases with only ferritic steel 18MND5 material properties Simonovski et al. (2014). Following this, different material zones were introduced into the specimens (Fig. 3) and a comprehensive benchmark, comparing results from several participants was performed Simonovski and Martin (2015); Simonovski et al. (2015).

Boundary conditions

The load to SEN(B) models was applied by moving the top pin downwards and prescribing contact between the pin and the specimen. The contact was defined as a ”hard contact”, meaning that the contact pressure is applied fully at the contact initiation, without any smoothing of the contact pressure. The default models use finite sliding contact implementation and do not use any friction. Pins were modelled as rigid surfaces and their displacements in the horizontal, vertical and rotational direction were prevented. Horizontal displacement of the models were prevented by fixing a node underneath the top pin in the horizontal direction.

The load to SEN(T) models was applied though reference points to the left and right of the models. Two boundary conditions were used: a) clamped and b) pin load type. For the clamped boundary conditions the rotations of the two references points were prevented and the rotational degree of freedom of the left and right specimen edges was tied to the rotational degree of freedom of the reference points. For the pin load boundary condition the left and right edges of the specimens were free to rotate. Rigid body movements of the models were prevented by fixing one node in the vertical and horizontal directions.

SEN(B): contact effects

The effects of the following contact parameters were explored: a) contact mesh density b) friction coefficient and b) finite versus small sliding contact implementation. Fig. 4 shows the effect of decreasing the mesh density underneath the contact surfaces by a factor of 0.5, 0.25, and 0.125 compared to the original contact mesh density. No significant effect can be observed on the J-integral values. However, the effect on the η_{pl} values is observable and η_{pl} increases by 3.4 % for the coarsest contact mesh density.

Fig. 5 shows the effect of friction coefficient value of μ=0, 0.01, 0.05 and 0.1 on the J-integral and η_{pl} values. There is practically no difference between μ=0 and μ=0.01 results. Increasing the friction coefficient to μ=0.05 decreases the J-integral values of almost 10 % at maximal load whereas η_{pl} values decrease only slightly (2.9 %). Using a friction coefficient of μ=0.1 further increases the loss of energy and therefore decreases the J-integral values by almost 20 % at maximal load. η_{pl} values decrease by 5.8 % compared to μ=0.

As can be seen in Fig. 6, the effect of finite versus small sliding contact implementation is quite substantial. Finite and small sliding contacts are both implemented using kinematic constraints with master and slave surface approach. An ‘anchor’ node on the slave surface is used to identify to which part of the master surface to transfer the load. In Fig. 6 the anchor node is indicatively given as node number 101. The load is transferred to the section of the master surface between nodes 201 and 202 as the node 101 lies between the two. This section is identified during the analysis. However, the small implementation does not update this section as the analysis proceeds. Such an approach is only valid if slave nodes slide less than an element length from their corresponding anchor point and are still in contacting with their local tangent plane Systemes (2014). If the master surface is highly curved, the slave nodes should slide only a fraction of an element length. Since the pins are sufficiently curved and the SEN(B) specimen slides between the bottom two pins as the load increases, neither of the conditions for small sliding is truly met. The finite sliding approach should be therefore used.

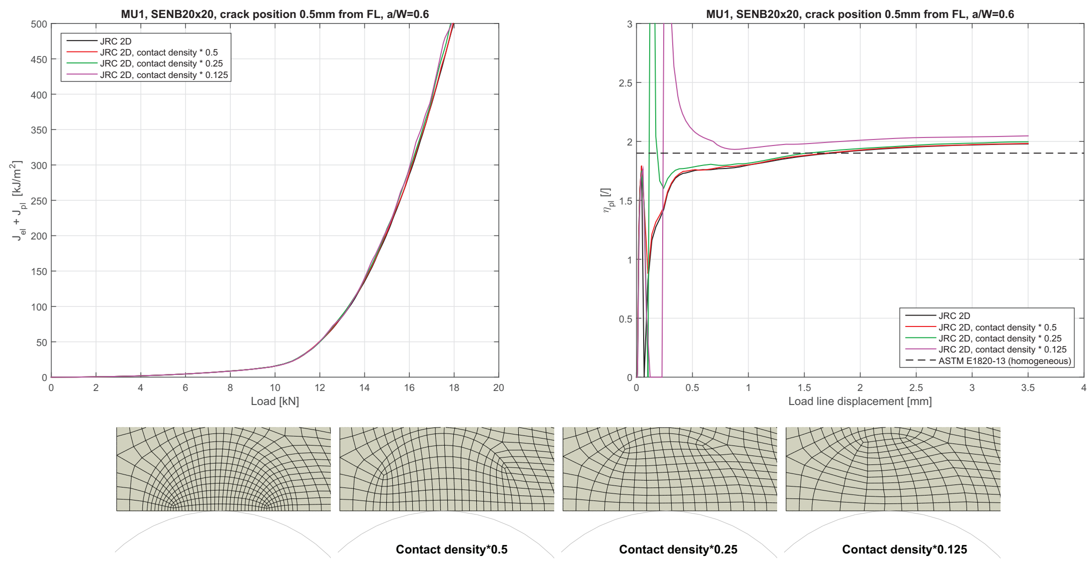

Figure 4: SEN(B)20x20, the effect of the pin contact mesh density.

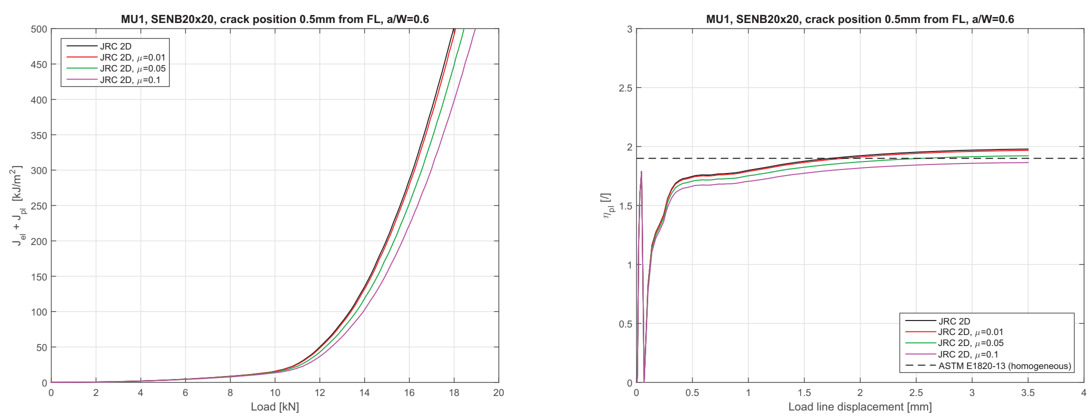

Figure 5: SEN(B)20x20, the effect of friction coefficient.

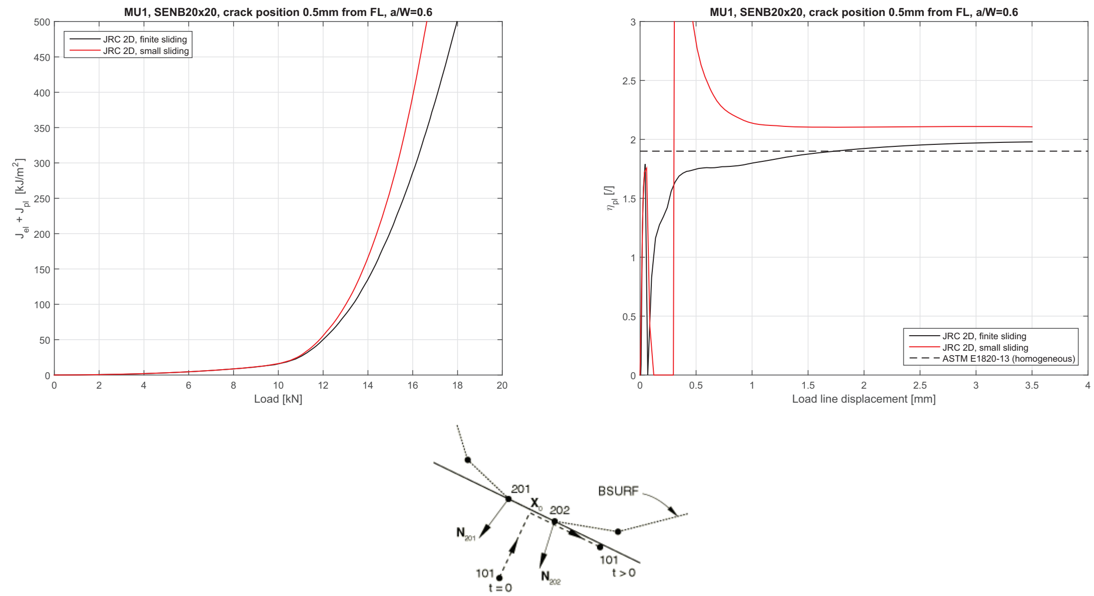

Figure 6: SEN(B)20x20, the effect of the finite and small sliding contact implementation.

SEN(B): weld angle and flipped weld

The sides of the weld in the mockup-up are not parallel but are at an angle of 2.7 °, Fig. 1. Since this is a relative small angle, a simplification can be done that the weld sides are parallel. Weld thickness can then be between 15 mm (the minimal width) and 18 mm (the maximal width). The impact of this simplification on J-integral and η_{pl} values is basically negligible, as shown in Fig. 7. Similarly, a crack can be placed in

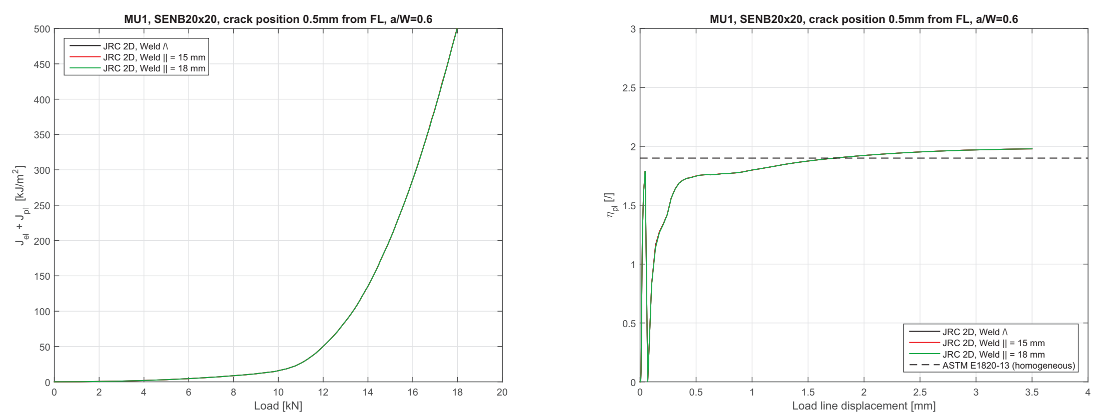

Figure 7: SEN(B)20x20, the effect of the weld angle simplification.

a weld, starting from the narrower or wider part of the weld, see Fig. 8. The latter case is referred here as the ‘flipped weld’. Since the weld angle does not have a significant effect, the effect of the flipped weld is also expected to be negligible. This is in fact confirmed by the results, Fig. 8. The red line (flipped weld) completely overlaps with the basic case.

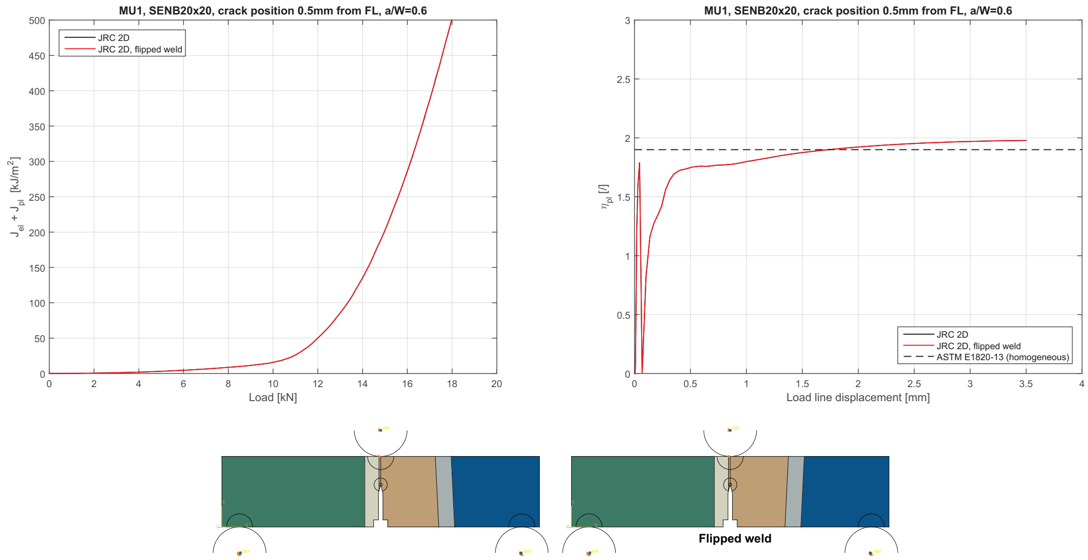

Figure 8: SEN(B)20x20, the effect of the flipped weld position.

SEN(T): clamped versus pin load

The effect of the clamped versus pin type of load conditions is on a SEN(T) specimen is shown in Fig. 9. Since clamped load conditions to a large extend prevent bending of the specimen around the crack line (compared to the pin load conditions), the un-cracked ligament is practically loaded in tension and less strain energy is generated around the crack tip. The corresponding J-integral values at a given load level are therefore considerably lower compared to the pin load. Interestingly, the calculated η_{pl} values for the pin load case are much closer to the DNV values of a homogeneous case.

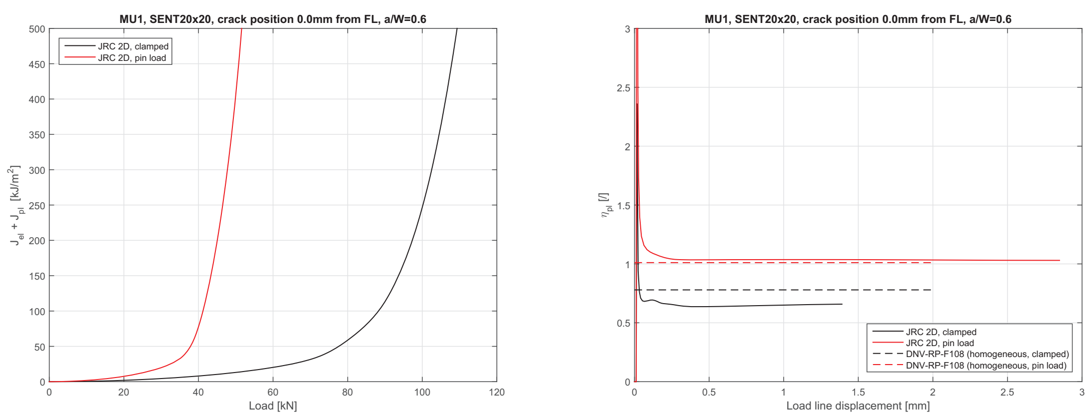

Figure 9: SEN(T)20x20, clamped versus pin load boundary conditions.

SEN(T): flipped weld

Figs.10 and 11 show the effect of the flipped weld on the computed J-integral and η_{pl} values for the clamped and pin load cases. Although flipped weld results in a slight difference for the clamped case only very minor differences can be observed for the pin load case.

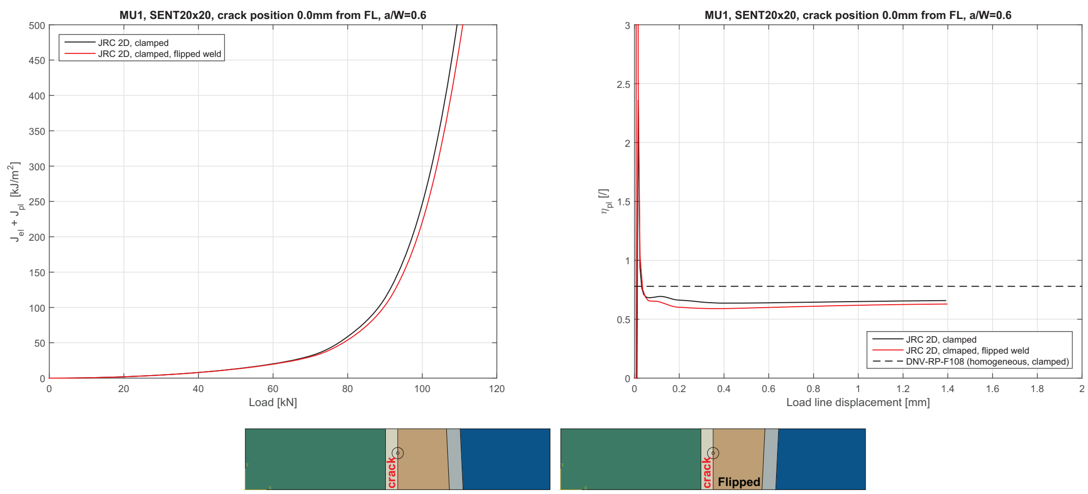

Figure 10: SEN(T)20x20, clamped boundary conditions, the effect of the flipped weld position.

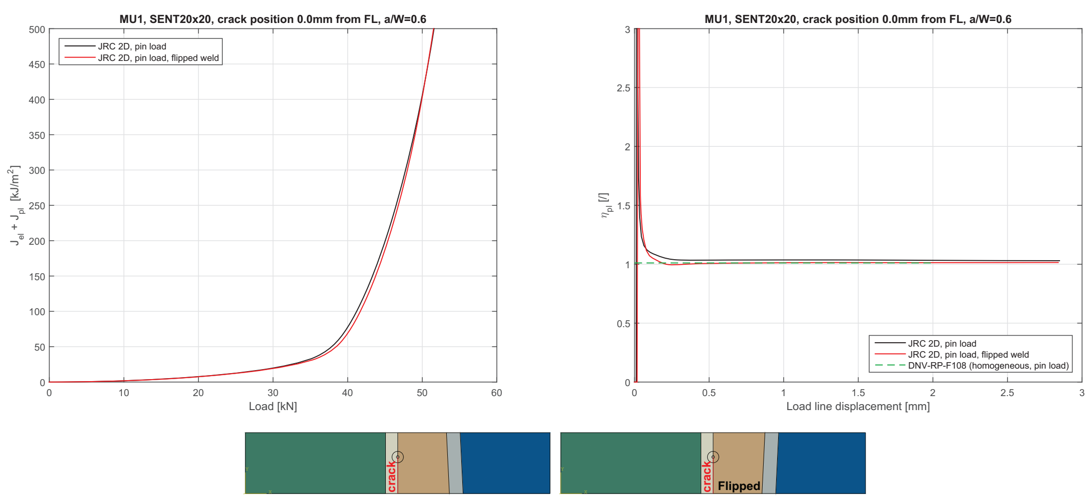

Figure 11: SEN(T)20x20, pin load, the effect of the flipped weld position.

CONCLUSIONS

J-integral fracture toughness and η_{pl} calculations were performed for EPR nuclear-grade welds between ferritic and austenitic stainless steel plates. Computations were performed on standard SEN(B) and SEN(T) specimens, each containing various dissimilar metal weld material zones. A systematic sensitivity analysis on the influence of various geometrical and modeling parameters on the computed J-integral and η_{pl} values was performed. The computations were performed within the MULTIMETAL project of the European Commission's 7th Framework Program.

For the SEN(B) specimens the parameter with the largest importance (in addition to a good global finite element mesh) was the selection of finite sliding contact implementation. This is preferable over the small sliding implementation since relative sliding of the surfaces in contact is larger than the size of the finite elements in the contact area. Friction is also important and can decrease the J-integral values of up to 20 % and η_{pl} by up to 5.8 %. Contact mesh density has almost no effect on the J-integral values but tends to increase the η_{pl} values. Simplifying the weld geometry by assuming parallel weld sides has basically no effect on the computed result nor does flipping of the weld.

For the SEN(T) specimens the parameter with the largest influence is the loading: clamped versus pin load. Flipping the weld has basically negligible effect.

ACKNOWLEDGMENTS

This project has received funding from the European Community's Seventh Framework Program (FP7/2012-2015) under grant agreement n°295968.

REFERENCES

ASTM. *Standard Test Method for Measurement of Fracture Toughness. E1820-13*. American Society for Testing and Materials (ASTM), 2013.

M. Bourgeois, O. Ancelet, and S. Chapuliot. Elasto-plastic properties in dissimilar metal weld junctions: Stress-strain curves determination for constitutive materials. In *Proceedings of the ASME 2015 Pressure Vessels and Piping Conference*. ASME, 2015a.

M. Bourgeois, O. Ancelet, G. Perez, P. Rózsahegyi, S. Szávai, and S. Lindqvist. MULTIMETAL Deliverable D3.6, Mechanical Behaviour Identification. Technical report, CEA, BZF, VTT, January 2015b.

M. Bourgeois, G. Perez, and S. Chapuliot. Fracture properties in dissimilar metal weld junctions: Experimental methodology of characterization. In *Proceedings of the ASME 2015 Pressure Vessels and Piping Conference*. ASME, 2015c.

W. Brocks and I. Scheider. Numerical aspects of the path-dependence of the J-integral in incremental plasticity. how to calculate reliable J-values in FE analyses. Technical report, Institut fur Werkstofforschung GKSS-Forschungszentrum Geesthacht, 2001.

DNV. *Recommended practice DNV-RP-F108. Fracture control for pipeline installation methods introducing cyclic plastic strain*. DET NORSKE VERITAS (DNV), 2006.

C. Faidy. Structural integrity of dissimilar welds: ADIMEW project overview (http://dx.doi.org/10.1115/pvp2004-2540). In *Proceedings of the ASME 2004 Pressure Vessels and Piping Conference*. ASME, 2015.

ISO. *ISO 12135:2002 Metallic materials - Unified method of test for the determination of quasistatic fracture toughness*. International Organization for Standardization (ISO), 2002.

H. Keinänen, P. Karjalainen-Roikonen, P. Gilles, E. Keim, S. Blasset, and T. Nicak. Results of EC FP7 structural performance of multi-metal component project: Dissimilar metal weld fracture resistance investigation. In *Proceedings of the ASME 2015 Pressure Vessels and Piping Conference*. ASME, 2015.

M. Kikuchi and H. Miyamoto. Evaluation of J_k integrals for a crack in multiphase materials. *Recent Research on Mechanical Behavior of Materials, Bulletin of Fracture Mechanics Laboratory*, 1, 1982.

O. Kolednik, J. Predan, G.X. Shan, N.K. Simha, and F.D. Fischer. On the fracture behavior of inhomogeneous materials-a case study for elastically inhomogeneous bimaterials. *International Journal of Solids and Structures*, 42(2):605–620, January 2005.

MULTIMETAL. 'Structural performance of multi-metal component' (http://projects.tecnatom.es/webaccess/multimetal), 2012.

N.K. Simha, F.D. Fischer, O. Kolednik, and C.R. Chen. Inhomogeneity effects on the crack driving force in elastic and elastic-plastic materials. *Journal of the Mechanics and Physics of Solids*, 51(1):209–240, January 2003.

I. Simonovski and O. Martin. MULTIMETAL Deliverable D4.2: J Value Estimation of Different Multi-Metallic Specimen Designs. Technical report, European Commission, Joint Research Centre (JRC), Institute for Energy and Transport, 2015.

I. Simonovski, O. Martin, and G. Machina. MULTIMETAL WP4.2: WP4.2 'K/J Value Estimation of different Specimen Designs' Part 1: Homogeneous Specimens. Technical report, European Commission, Joint Research Centre (JRC), Institute for Energy and Transport, 2014.

I. Simonovski, M. Oliver, M. Bourgeois, M. Aït-Bachir, S. Szabolcs, R. Beleznai, O. Costa Garrido, L. Cizelj, S. Blasset, E. Jourden, C. C.-F. García, and G. L. Quesada. J-integral fracture toughness assessment of specimens containing dissimilar metal welds. In *Proceedings of SMiRT-23 Conference*. IASMiRT, 2015.

STYLE. 'Structural integrity for lifetime management-non rpv components', grant agreement no 249648, 2010.

Dassault Systemes. *ABAQUS 6.14-2 (http://www.simulia.com/)*, 2014.